Supplementary Information for:

The conical shape of DIM lipids promotes *Mycobacterium tuberculosis* infection of macrophages

Jacques Augenstreich, Evert Haanappel, Guillaume Ferré, Georges Czaplicki, Franck Jolibois, Nicolas Destainville, Christophe Guilhot, Alain Milon*, Catherine Astarie-Dequeker*, Matthieu Chavent*

* Correspondence should be addressed to M.C. (email: matthieu.chavent@ipbs.fr), to C.A.-D. (email: catherine.astarie-dequeker@ipbs.fr), or to A.M. (email: alain.milon@ipbs.fr)

This PDF file includes:

- Supplementary materials and methods
- Supplementary text
- Tables S1 to S3
- Figures S1 to S11
- Caption for movie S1
- SI reference citations

Other supplementary materials for this manuscript include the following:

Movie S1

SUPPLEMENTARY MATERIALS AND METHODS

Lipid analysis by MALDI-TOF MS analysis

DIM were analyzed by matrix-assisted laser desorption-ionization time-of-flight (MALDI-TOF) mass spectrometry, as described previously (1). Lipid residues were dissolved in 20 µL of $CHCl_3$, deposited on the analysis plate and dried. Then, 0.5 µL of 2,5-dihydroxybenzoic acid (10 mg/mL) dissolved in $CHCl_3/CH_3OH$ (1:1, vol:vol) were deposited on the sample and allowed to crystallize at room temperature. Mass spectra were acquired with a MALDI TOF/TOF 5800 analyzer (Applied Biosystems/AB SCIEX, Framingham, MA, USA) equipped with an Nd:YAG laser (Wavelength 349 nm; pulse rate 400 Hz). The acquisition was carried out in continuous scan mode, in positive mode with a laser intensity of 3500 (arbitrary unit of the software). The final spectrum was obtained by accumulating 10 spectra of 250 laser shots.

Formation of multilamellar vesicles for HRMAS NMR experiments

To form multilamellar vesicles (MLV) of well-defined lipid compositions, we mixed appropriate volumes of chloroformic stock solutions of the different lipids in glass tubes. The chloroform was evaporated using a rotating evaporator. We inclined the tubes in the evaporator, resulting in the formation of a thin lipid film over a large area of the tube. The lipids were further dried under vacuum for ~2 h to remove any remaining traces of the solvent. Next, we added sufficient Tris buffer (10 mM Tris, 1 mM EDTA, pH 7.4) to the tubes to cover the lipid film. The lipids were left to hydrate at a temperature chosen to favor the formation of the lamellar phase of the liposome membranes (see SI for further details). We then vortexed each tube 6 × 30 s. After vortexing, we obtained a cloudy suspension of liposomes. We transferred the liposome suspensions to 1.5 mL centrifuge tubes and centrifuged the tubes for 15 min at 16000 g, then stored them at 4°C. Before each NMR experiment, we removed the supernatant and transferred 50 µL of the liposome pellet to a 4 mm MAS rotor, taking care not to warm the liposomes. Before introducing the rotor into the NMR spectrometer, we equilibrated the temperature to ~5°C.

In order to be sure to prepare the membranes in the lamellar phase, we adapted the temperature of hydration to the lipid composition. Pure DOPE has a lamellar-to-inverted-hexagonal transition temperature of 10°C. Accordingly, we hydrated the samples of DOPE, DOPE/SOPC (9:1) and DOPE/SOPC (5:1) for 15 min on ice. We

vortexed the lipids 6 × 30 s (with cooling on ice for at least 30 s between vortexing periods) in order to prepare and conserve the liposomes in the lamellar phase. DOPE/SOPC (3:1), DOPE/SOPC (1:1) and pure SOPC (which do not form a H_{II} phase at 30°C) were incubated at 30°C in a water bath and vortexed 6 × 30 s with return to the water bath.

Incorporating the highly hydrophobic lipid DIM into liposomes requires incubating the lipids at higher temperature, but this would have favored the formation of the inverted-hexagonal phase for some membrane compositions. We therefore adapted our protocol for DIM-containing liposomes and their controls without DIM. For these lipid mixtures, we hydrated the lipids at 37°C on a shaker overnight. We then transferred the tubes to a water bath set at 37°C. The tubes were vortexed for 6 × 30 s, with return to the water bath between vortexing periods. All liposomes with compositions DOPE/SOPC (3:1) +/- DIM, DOPE/SOPC (3:1) +/- TAG and DOPE/SOPC/lysoPC (75:20:5) +/- DIM were prepared according to this protocol. We checked the correct incorporation of DIM in the liposomes using thin-layer chromatography on a few µL of the liposome suspension. We also conducted a separate ^{1}H-NMR experiment to quantify the incorporation of DIM in liposomes using our protocol.

Bacterial strains and growth conditions

The strains used in this study included the wild-type (WT) *M. tuberculosis* strain, H37Rv Pasteur (the sequenced strain from Institut Pasteur, Paris) and two distinct H37Rv mutants. The *ppsE* mutant (H37RvΔ*ppsE*) was constructed in a previous study by insertion/deletion within the polyketide synthase gene *ppsE* (2) required for the synthesis of DIM. The WT strain and the H37RvΔ*ppsE* mutant were rendered fluorescent by the transfer of plasmid pMV361H *gfp* (3). The *lppX mutant (*H37Rv Δ*lppX)* was constructed by homologous recombination using the thermosensitive counterselectable plasmid pPR27 as previously described (4). Briefly, a 2.6kb DNA fragment covering the *lppX* gene was amplified by PCR from H37Rv genomic DNA using primers lppXA (5'-GCTCTAGAGTTTAAACGCATTTGAGCAGCCGAG-3') and lppXB (5'-GCTCTAGAGTTTAAACGAAGAATACCTGGCCGC-3') and inserted into a cloning vector. The *res-Ωkm-res* cassette was inserted at the unique KpnI site within the *lppx* gene to generate the allelic exchange substrate (AES) formed of the *res-Ωkm-*

res cassette flanked by two arms (of approximately 1kb) specific to *lppX*. This AES was recovered on a PmeI restriction fragment and inserted into the XbaI site of pPR27. The resulting plasmid was transferred into the recipient *M. tuberculosis* H37Rv strain and allelic exchange mutants were selected as described previously (4). Kanamycin and sucrose resistant clones were analyzed by PCR using primers lppXC (5'-CAAACGCGTTTCTGGACGG-3'), lppXD (5'-GGCAATCCACACGGTCGC-3'), lppXE (5'-GAGCATTGAAAGCTCCCACC-3') specific of the *M. tuberculosis* H37Rv genome, and res1 (5'-GCTCTAGAGCAACCGTCCGAAATATTATAAA-3') and res2 (5'-GCTCTAGATCTCATAAAAATGTATCCTAAATCAAATATC-3') specific of the *res-Ωkm-res* cassette. One clone giving the pattern corresponding to the allelic exchange was retained for analysis and named H37Rv Δ*lppX (or PMM76).*

All strains were cultured at 37°C in Middlebrook 7H9 liquid medium (BD Difco) containing 10% albumin-dextrose-catalase (ADC) (BD Difco). When required, kanamycin, hygromycin and Tween-80 were added to the medium to a final concentration of 40 µg mL^{-1}, 50 µg mL^{-1} and 0.05% (v/v) respectively.

Purification of DIM and preparation of lipid solutions

DIM were purified from *M. canetti* as previously described (5). Briefly, total mycobacterial lipids were extracted from stationary cultures of *M. canetti*. The bacteria were left successively in $CH_3OH/CHCl_3$ (2:1, vol/vol) for 48 h and in $CH_3OH/CHCl_3$ (1:2, vol/vol) for 24 h. The organic phase was recovered, washed with water and dried. Total lipids were then resuspended in $CHCl_3$ and the chromatographic separation of DIM was run manually using Sep-Pak Silica Classic Cartridges (55-105 µm particle size; Waters) and an elution gradient of an increasing concentration of diethylether (0-10% (v/v)) in petroleum ether. Fractions containing the isolated compounds were pooled and dried.

Stock solutions of purified DIM (40 mg/mL), POPE (20 mg/mL) and POPC (21 mg/mL) were prepared by dissolving the dried lipids in $CH_3OH/CHCl_3$ (2:1, vol/vol). The solutions were then injected in serum-free RPMI 1640 medium (Gibco) at the final concentration of 70 µM (1/400 dilution) and sonicated at 37°C until complete dispersion of the lipids.

Macrophage culture

The human promonocytic cell line THP-1 (ECACC 88081201; Salisbury, UK) was cultured in RPMI 1640 medium containing 10% heat-inactivated fetal bovine serum (FBS), 2 mM L-Glutamine, 1 mM sodium pyruvate, and 1% MEM non-essential amino acids. For macrophage differentiation, the THP-1 cells were washed and suspended in medium containing 10% FBS. The cells were distributed in a glass petri dish at a density of 3 x 10^6 cells/petri dish and were differentiated into macrophages with 30 nM phorbol 12-myristate 13-acetate (PMA) for 3 days. Before use, the cells were washed twice with fresh medium.

Human blood purchased from the Etablissement Français du Sang in Toulouse (France) was collected from fully anonymous non-tuberculous donors. Human macrophages derived from monocytes (hMDMs) were prepared as previously described (3). Briefly, monocytes were isolated from peripheral blood mononuclear cells (PBMC) by adhesion on a glass coverslip in 24-well tissue culture plates. Monocytes (5 x 10^5 cells/well) were differentiated into human monocyte-derived macrophages (hMDMs) in RPMI 1640 (Gibco), supplemented with 2 mM glutamine (Gibco) and 7% (v/v) heat-inactivated human AB serum for 7 days.

Macrophage infection

Single bacterium suspensions were prepared with exponentially growing strains as previously described (3). Briefly, the bacteria were grown to mid-exponential growth phase on Middlebrook 7H9 liquid medium supplemented with 10% ADC, and were then pelleted by centrifugation and dispersed in serum-free RPMI 1640 medium using glass beads. The number of bacteria per mL in the suspension was estimated by measurement of the optical density at 600 nm. The bacteria or zymosan particles were added to the macrophages at the indicated multiplicity of infection (MOI) and incubated for 1-2 h at 37°C in an atmosphere containing 5% CO_2. Extracellular bacteria or particles were removed by three successive washes with fresh medium.

Assay for monitoring DIM transfer to macrophage membranes

For experiments with purified DIM, THP-1 cells were incubated with RPMI 1640 medium supplemented with 70 µM DIM at 37 °C and 5% CO_2. After 1 h, the cells were rinsed with fresh medium and detached by incubation with a 0.05% trypsin-EDTA

solution (Gibco) for 15 min. The cells were then harvested, centrifuged at 150 x g for 10 min and the cell pellet was suspended in RPMI 1640 medium (A).

For experiments with DIM in the context of the *M. tuberculosis* cell envelope, THP-1 cells were incubated with H37Rv WT or H37Rv Δ*lppX* (MOI 15:1), washed with fresh RPMI-1640 medium, and further incubated in the presence of serum at 37°C and 5% CO_2. After 40 h, the cells were rinsed with RPMI-1640 medium, detached enzymatically with trypsin and centrifuged at 150 x g for 10 min. The membranes were prepared using a protocol adapted from Rhoades *et al*. (6). The pellet was suspended in 1 mL ice-cold homogenization buffer (1 mM EDTA, 20 mM HEPES, pH 7) containing 250 mM sucrose and the cells were disrupted by 25 passages through a 26-gauge needle. Following centrifugation at 3,000 x g for 10 min at 4°C in order to sediment nuclei and large cell debris, the supernatant was recovered. This step was repeated twice. The supernatant was layered onto a linear gradient of 30% to 12% sucrose and centrifuged at 2,000 x g for 1 h at 4°C. The upper portion of the gradient containing the membrane fraction was isolated, layered on a discontinuous gradient of 50% to 25% sucrose, and centrifuged at 2,000 x g for 30 min at 4°C. The fraction above the 25% portion containing the membrane fraction was isolated, centrifuged at 110,000 x g for 1 h at 4°C and the membrane pellet was taken up in homogenization buffer (B).

Total lipids were extracted from the macrophage membranes using the Bligh and Dyer extraction protocol (7). Briefly, to one volume of cells suspension (A) or membrane fraction (B), 2.5 volumes of CH_3OH and 1.25 volumes of $CHCl_3$ were added. The mixture was incubated at room temperature for 48 h. Then, 1.25 volumes of $CHCl_3$ followed by 1.25 volumes of $CHCl_3$ were added. This mixture was left standing for 24 h to separate the organic and aqueous phases. Twenty-four hours later, the organic phase containing the lipids was recovered and dried under a stream of nitrogen. For the membrane fraction samples, the DIM were purified from the total lipid extract by column chromatography using a Florisil column. The Florisil was equilibrated with a solution of petroleum ether/diethyl ether (98:2, v/v). The total lipid extract was dissolved in this solution and DIM were eluted with the same solution.

Phagocytosis assay

Phagocytosis was assessed as described previously (3). Briefly, human monocyte-derived macrophages (hMDMs) were infected with GFP-expressing bacteria (MOI 10:1) or zymosan (MOI 30:1) for 1 h. When indicated, the hMDMs were

pre-treated for 1 h with 70 µM lipids or 1/400 lipid solvent ($CH_3OH/CHCl_3$ (2:1, vol/vol) prepared in RPMI as for lipid suspension). At the end of infection, the hMDMs were intensively washed and fixed with 4% (w/v) PFA. For mycobacteria, extracellular GFP-bacilli were labelled with rabbit anti-mycobacteria Ab revealed by a Rhodamine Red-conjugated goat anti-rabbit secondary Ab. The cells were then stained for 15 min with WGA conjugated to Alexa Fluor® 350. For zymosan, the hMDMs were permeabilized with 0.3% Triton X-100 for 5 min and labelled with TRITC-phalloidin. Extracellular zymosan was readily distinguished from internalized particles, which appeared as yellowish grains within a dark phagosome bordered by diffuse red staining. The percentage of cells having ingested at least one bacterium or zymosan particle was determined by fluorescence microscopy using a Leica 43 DM-RB epifluorescence microscope. For each set of conditions, the experiments were performed in duplicate and at least 100 cells were counted per slide. Data are presented as the mean ± standard error of the mean (SEM) of the indicated number of experiments (n). Data were analyzed by the Wilcoxon signed-rank test using GraphPad PRISM (GraphPad Software, GPW5-078069-NBH9780) and $p < 0.05$ was used as the limit of statistical significance.

Quantum mechanics

To calculate partial charges for DIM lipid, a molecular dynamics simulation was first performed for 40 ns in the NPT ensemble. Lipid14 (8) and general AMBER force field (Gaff) (9) were used in order to describe bonded and non-bonded terms within the AMBER program. From this trajectory, 30 structures were extracted based on the clustering method (*kclust* from the MMTSB Toolkit, with the radius of 2.5 Å). These structures were fully optimized at the HF/6-31G* quantum chemical method using the Gaussian 09 suite of programs (http://gaussian.com/). Partial charges were then obtained using RESP method (10) (RESP-A1) implemented in the RED tools (11). For each structure, partial charges where obtained by charge fitting to the electrostatic potential at points selected according to the Merz-Singh-Kollman scheme (12, 13) as proposed by the RESP-A1 method. Before charge calculations, a reorientation procedure was applied in order to maintain one ester (O=C-O) group in the same orientation for all 30 structures. Partial charges for the head groups of the DIM model are displayed in Figure S2.

SUPPLEMENTARY TEXT

Tilt angle analysis and curve fitting

The lamellar to inverted hexagonal phase transition was characterized from the coarse-grained (CG) simulations data by analyzing the distributions of the local orientations of SOPC and DOPE. The orientations of these molecules are described by the tilt angle θ between their director (*i.e*. the principal axis of the inertia tensor) and the z-axis of the CG simulation space (aligned with the membrane normal in the lamellar phase). When $\theta > \pi/2$, we use $\theta' = \pi - \theta$ to uniformly describe the lipid orientation for the two membrane leaflets. Lipid orientation distributions were obtained by counting molecules in 100 bins of width $\delta\theta = \pi/200$ from 0 to $\pi/2$ for the last 250 frames of the CG simulations of pure SOPC at 310 K, pure DOPE at 350 K, and DOPE/ SOPC/DIM mixtures at several temperatures, except with 2.5% DIM at 340 K where the last 125 frames were used (due to a late transition). The distributions were then normalized by their integral as evaluated from molecule and frame numbers.

Lamellar phase: In the lamellar phase, due to periodic boundary conditions, the bilayers are globally parallel to the (xOy) plane and normal to the (Oz) axis. The director of each lipid is on average parallel to (Oz). The local orientation is expressed by the lipid's polar angle $\theta \in [0, \pi/2]$. We assume that the deviation from the normal orientation is described by a simple elastic model with an energy given by $E(\theta) = -\kappa_1 \cos\theta$, where κ_1 is a bending elastic modulus, similar to an electric dipole in an external field**.** With this expression for the energy $E(\theta)$, the equilibrium Boltzmann distribution of the angle θ at temperature T is given by the equation:

$$p_{\text{lam}}(\theta) = \frac{1}{Z} \sin\theta \, e^{\tilde{\kappa}_1 \cos\theta} \quad \text{(Eq. S1)}$$

where $Z = (e^{\tilde{\kappa}_1} - 1)/\tilde{\kappa}_1$ is the normalization factor and $\tilde{\kappa}_1 = \kappa_1/(k_B T)$, $k_B T$ being the thermal energy. The reference distribution function of the lipid orientation in the lamellar phase was obtained by fitting CG data of SOPC at 310 K with Eq. S1, as illustrated in the figure below where the fitted value is $\tilde{\kappa}_1 \simeq 12$.

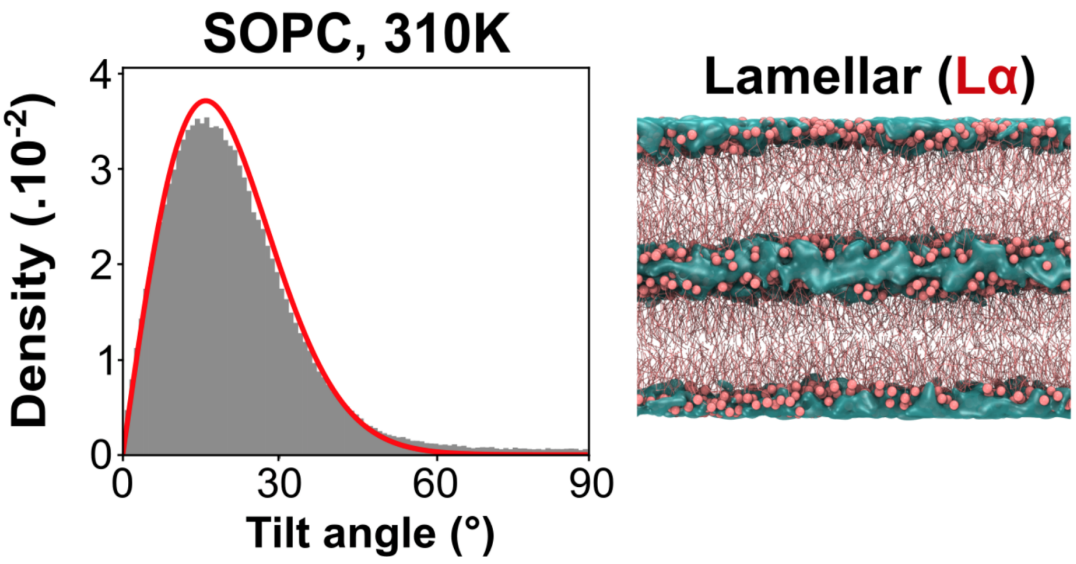

Distribution of lipid orientations in the lamellar phase. Left: Histogram (in gray) of tilt angles θ extracted from CG simulations. The red curve is a fit to the probability distribution $p_{lam}(\theta)$ (Eq. S1) given in the text with $\tilde{\kappa}_1 \simeq 12$. Right: Lamellar SOPC system used for the fit.

When the lamellar and hexagonal phases coexist, as discussed in the main text, the bilayers are not as regular as in the pure lamellar phase. One type of possible perturbation is that the bilayers are tilted with respect to the normal orientation $\theta = 0$, by an average angle $\theta_0 > 0$. To simulate this effect, angles θ were sampled as follows (see figure below, upper left): a fixed vector making an angle θ_0 with (Oz) is defined and sampled lipid directors make an angle θ' with it following the same distribution as in equation S1. The angles θ that these lipid directors make with (Oz) are then calculated. We have tested a simple phenomenological fitting law:

$$p_{\text{lam},2}(\theta) = \frac{\beta}{Z} \sin\theta \, e^{\kappa_1 \cos(\theta-\theta_0)/k_B T} \qquad \text{(Eq. S2)}$$

that gives very satisfactory fits, but with a fitted parameter $\theta_{0,\text{fit}}$ different from the original value θ_0, as shown in the table below. Note that, in addition, the normalization factor $1/Z$ must be rescaled by a prefactor β to ensure that the total probability remains equal to 1.

θ_0 (°)	10	15	20	24	30	40
$\theta_{0,\text{fit}}$ (°)	4	8	13	19	26	37
β	0.75	0.57	0.42	0.33	0.26	0.19

Fitting parameters table. Values of the fitted parameters $\theta_{0,\text{fit}}$ and β for given tilt angles θ_0 for $\tilde{\kappa}_1 \simeq 12$. Angles are given in degrees.

When fitting the simulated data, one measures the angle $\theta_{0,\text{fit}}$. From its value, the prefactor β must be inferred. For this, we propose the following interpolation function, based on the values in the table above for $\tilde{\kappa}_1 = 12$:

$$\beta(\theta_{0,\text{fit}}) \simeq 0.67e^{-0.11\theta_{0,\text{fit}}} + 0.33e^{-0.015\theta_{0,\text{fit}}} \qquad \text{(Eq. S3)}$$

Inverted hexagonal phase: An ideal inverted hexagonal phase is made of parallel cylinders whose axes form a hexagonal array. If the distance between these cylinders is sufficiently large, the orientation of lipids is isotropic around each cylinder. As illustrated in the figure above (upper right), the average orientation of a lipid director is perpendicular to the cylinder surface. We denote by γ the corresponding polar angle, as displayed in the figure. As in the lamellar phase, we assume that due to thermal fluctuations, lipid directors actually make an angle θ' with this average orientation with a probability distribution $p(\theta') = \frac{1}{Z} \sin\theta' \, e^{\tilde{\kappa}\cos\theta'}$. We again sampled angles θ by drawing a random angle γ uniformly on $[0,2\pi[$ and a random angle θ'. We successfully fitted the obtained data with the following heuristic law, where $Z_{\text{hex},0}$ is a normalization factor:

$$p_{\text{hex},0}(\theta) = \frac{1}{Z_{\text{hex},0}}\left[1 - e^{-\frac{\theta}{\tilde{\kappa}_{21}}}\cos\left(\frac{\theta}{\tilde{\kappa}_{22}}\right)\right] \qquad \text{(Eq. S4)}$$

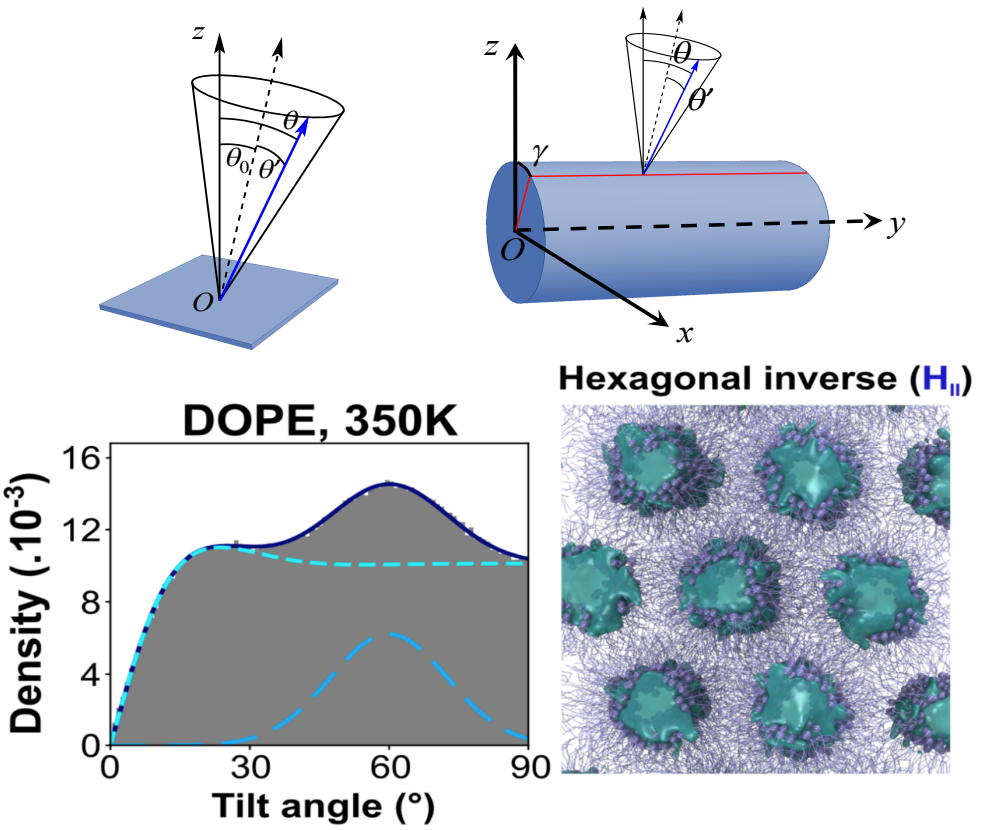

Distribution of lipid orientations in the inverted hexagonal phase. Upper left: In the lamellar phase case, construction of a lipid director (blue arrow) isotropically distributed around a fixed tilt direction with polar angle θ_0 (dashed arrow). The membrane is represented by the blue plane parallel to (xOy). Upper right: The hexagonal phase is made of parallel lipid cylinders (in blue) with axes chosen here to be parallel to the (Oy) axis, without loss of generality. For a given lipid, its director is on average normal to the cylinder surface (dotted arrow). It is characterized by the polar angle $\gamma \in [0,2\pi[$. The lipid director (blue arrow) is isotropically distributed around this average direction. Lower left: Histogram (in gray) of tilt angles θ (in degrees) from MARTINI simulations. The dark blue solid curve is a fit with the probability distribution $p_{\mathrm{hex}}(\theta)$ (Eq. S2) given in the text. The cyan dashed line is the probability distribution $p_{\mathrm{hex},0}(\theta)$ if the hexagonal phase were ideal. The blue long-dashed line represents favored areas for lipid tails in between the water tubes (see text below). Lower right: hexagonal DOPE system used for the fitting.

When the distance between cylinders decreases, the lipid tails in opposing cylinders of the inverted hexagonal phase H_{II} repel each other. Some director orientations are favored in coherence with the hexagonal symmetry perpendicularly to the cylinder axes (as already seen by others (14)). To mimic this fact, we again propose a heuristic law by adding a Gaussian distribution to the previous one:

$$p_{\mathrm{hex}}(\theta) = \frac{(1-c)}{Z_{\mathrm{hex},0}}\left[1 - e^{-\frac{\theta}{\tilde{\kappa}_{21}}}\cos\left(\frac{\theta}{\tilde{\kappa}_{22}}\right)\right] + c\,\frac{1}{\sqrt{2\pi}\sigma}\exp -\left[\frac{(\theta-\theta_1)^2}{2\sigma^2}\right] \quad \text{(Eq. S5)}$$

where $0 \leq c \leq 1$ is the weight of the Gaussian correction, which has a mean value $\theta_1 = \pi/3$ and a standard deviation σ. The reference orientation distribution function of the inverted hexagonal phase was obtained by fitting CG data of DOPE at 350K with Eq.

S5. Due to the important number of parameters to be fitted in this equation, the fits were performed with an program developed in-house for stochastic global optimization by simulated annealing (GOSA) (15). This method allows improving the quality of the fit in the case of a high dimensionality of the parameters space, compared to deterministic gradient-based algorithms such as steepest descent or conjugate gradients. Fitting of the tilt angles in the inverted hexagonal phase (lower left figure) illustrates how well this heuristic law fits the distribution extracted from CG simulations.

Coexistence of lamellar and inverted hexagonal phase:

The distribution of lipid orientations for the DOPE/SOPC/DIM mixture in the CG simulations were fitted with a linear combination of the reference distribution functions given previously (Eq. S1 and S5):

$$p_{mix}(\theta) = A\left[\frac{\beta(\theta_0)}{Z}\sin\theta\, e^{\tilde{\kappa}_1\cos(\theta-\theta_0)}\right] + (1-A)\left[\frac{(1-c)}{Z_{\text{hex},0}}\left[1 - e^{-\frac{\theta}{\tilde{\kappa}_{21}}}\cos\left(\frac{\theta}{\tilde{\kappa}_{22}}\right)\right] + c\,\frac{1}{\sqrt{2\pi}\sigma}\exp-\left[\frac{(\theta-\theta_1)^2}{2\sigma^2}\right]\right] \quad \text{(Eq. S6)}$$

by using GraphPad Prism 5.04 (GraphPad Software, La Jolla California USA). As described above, the tilt angle θ_0 and the rescaled prefactor $\beta(\theta_0)$ were introduced because of perturbations due to phase coexistence. It permits to determine the percentage, A, of the lamellar phase contribution for DOPE and SOPC lipids separately in each CG simulation using the values of $\tilde{\kappa}_1, c, Z_{\text{hex},0}, \tilde{\kappa}_{21}, \tilde{\kappa}_{22}$ and σ resulting of fitting the reference functions for the lamellar and inverted hexagonal phase. See Figure below for an illustration of the fitting for a tilt angle distribution of DOPE.

Phase transition curves were finally obtained by fitting a sigmoid function to the variation of A as a function of temperature for each DOPE/SOPC/DIM mixture using Eq. S7 where A_0 and T_{50} respectively stand for the initial lamellar phase contribution and the phase transition midpoint temperature, while k is linked to the slope of the function at T_{50}. The same equation was used to fit phase transitions monitored by ^{31}P NMR.

$$A(T) = A_0\,\frac{1}{1+\exp[-k\,(T-T_{50})]} \quad \text{(Eq. S7)}$$

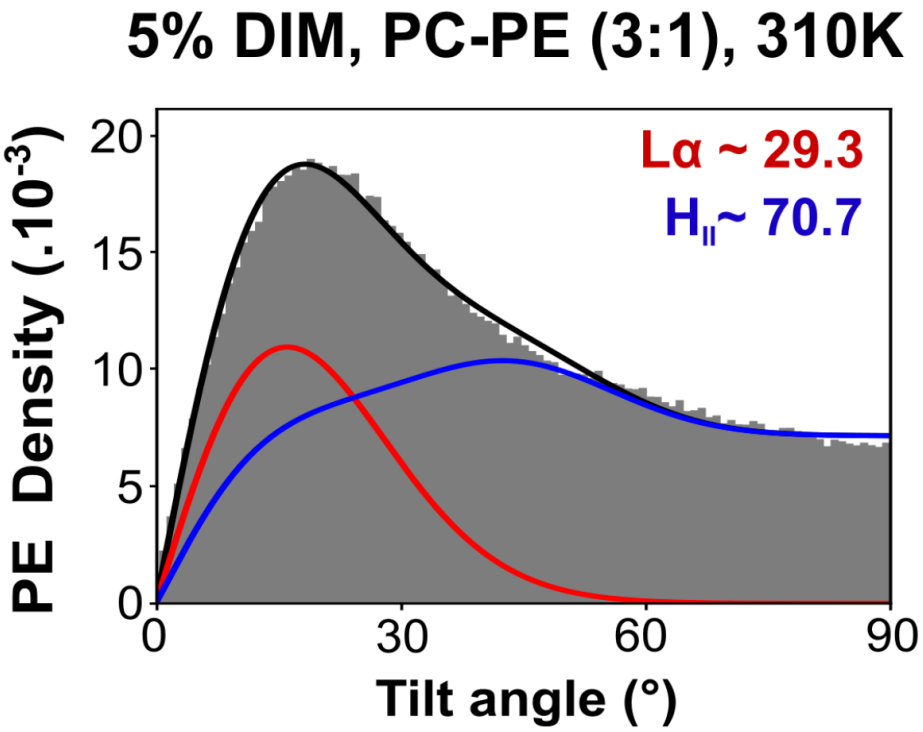

Distribution of lipid orientations in a mixed-phase system. DOPE tilt angle distribution for a system containing both inverted hexagonal and lamellar phases (see Fig. 3b). Fitting of the complete distribution (Eq. S6) in black. Individual contributions of lamellar and inverted hexagonal phases in red and blue, respectively.

DIM quantification in liposomes

To assess the quantity of DIM incorporated in freshly prepared liposomes, and whether this concentration stayed stable over time, we measured the percentage of DIM actually inserted into liposomes prepared with different percentages of DIM, and equilibrated for several durations and temperature.

Using the protocol for the formation of multilamellar vesicles (see Methods), we formed two batches of liposomes of DOPE and SOPC (3:1) containing 1%, 2.5% and 5% (mol/mol) of DIM, respectively. Each liposome batch contained 100 µg of DIM and appropriate masses of DOPE and SOPC for the targeted DIM percentage. We split each liposome batch into two equal volumes, which we transferred into plastic microcentrifuge tubes (Eppendorf). For each batch, we immediately recovered the liposomes from one tube; we stored the other tube for 24 h at 37°C before recovering the liposomes. To recover the liposomes, we transferred the contents of each tube into a clean microcentrifuge tube. We centrifuged the tube for 15 min at 16000 g, discarded the supernatant and resuspended the pellet in 500 µL of ultrapure water (Milli-Q, Millipore). We then transferred the liposome suspension to a clean glass tube. The lipid suspensions were frozen in liquid N_2 and freeze-dried for 24 h.

We dissolved the dried lipids in 250 µL of $CDCl_3$ and transferred the lipid solutions into ∅3 mm NMR tubes. We measured the liquid-state ^1H NMR spectra of all six tubes on a Bruker 600 MHz spectrometer equipped with a TCI cryoprobe. To measure the DIM/phospholipid molar ratio for each condition, we identified characteristic well-separated peaks in the NMR spectra corresponding to DIM and to the phospholipids. For DIM, we used the quintuplet at 4.84 ppm corresponding to a DIM methine proton. For the phospholipids, we used peaks around 5.34 ppm corresponding to the ethylene protons in the DOPE and SOPC unsaturated side chains. We integrated these peaks and compared the areas to calculate the percentage of DIM in the lipids mixtures. The results of this quantification are shown in the table below. We conclude that, within experimental errors, the measured percentages of DIM agree with the calculated percentages, indicating a good incorporation of DIM into the liposomes prepared following our protocol. Moreover, we did not observe a decrease in the percentage of DIM after 24 h incubation, indicating that there is no exclusion of DIM from the liposome membranes.

Using the same method, we also measured the percentage of DIM in the liposomes of POPC/POPE/cholesterol/sphingomyelin (4:3:2:1) and POPE/cholesterol/ sphingomyelin (7:2:1) incorporating 5% of DIM by design. We removed the liposomes from the MAS rotor after the ^{31}P NMR experiment and recovered the lipids by freeze-drying. We found that the liposomes with composition POPE/cholesterol/sphingomyelin (7:2:1) indeed contained ~5% of DIM as expected. Surprisingly, the liposomes with composition POPC/POPE/cholesterol/sphingomyelin (4:3:2:1) contained only ~2.5% of DIM. This may indicate a reduced solubility of DIM in such type of membranes.

Quantification by ^{1}H-NMR of the percentage of DIM in freshly prepared liposomes and in liposomes stored for 24 h at 37°C.

Target percentage of DIM	Measured percentage of DIM	
	0 h	24 h, 37°C
1 %	0.81 %	0.89 %
2.5 %	2.8 %	2.2 %
5 %	5.2 %	5.5 %

Determination of lipid phase transition temperatures by ^{31}P NMR

Phosphorus NMR has been recognized for a long time as an excellent technique for identifying non-lamellar phases in lipid bilayers (16) and characterizing the dynamics of the phospholipid head groups (17). In every lipid phase, the phosphate nucleus is subject to specific movements that average its static chemical shift anisotropy (CSA) tensor in a specific way, thus producing a characteristic spectrum. The ^{31}P CSA of a liposome preparation can be measured in a static probe from its powder spectrum. Under magic angle spinning at a rate slower than the CSA width, the powder spectrum splits into spinning sidebands, from which the CSA parameters can be extracted (18). This approach has several advantages: it increases the resolution and sensitivity of the experiment, and allows analysing several CSA's in a lipid mixture, as long as the phosphorus atoms in the different head groups have distinct isotropic chemical shifts, which is the case for SOPC and DOPE.

Several lipid mixtures containing varying DOPE:SOPC molar ratios (1:0, 9:1, 5:1, 3:1, 1:1, 0:1) were investigated (see Table S2). As expected, decreasing the proportion of DOPE increased the lamellar (L_α) to inverted-hexagonal (H_{II}) phase transition temperature (19). Pure DOPE is already in the H_{II} phase at 5°C, the 9:1 and 5:1 mixtures have midpoint transitions at 24°C and 39°C, respectively, while the 3:1, 1:1 and 0:1 DOPE:SOPC mixtures do not transit to the H_{II} phase below 51°C, the highest temperature tested. In order to investigate the tendency of an extraneous lipid to induce a L_α to H_{II} transition, we focussed on a DOPE to SOPC ratio of 3:1 since the lipid membrane remains in the lamellar phase for this composition within the 9°C to 51°C temperature range, but is on the verge of a transition to the H_{II} phase. With this selected 3:1 ratio, we tested the effect of adding small amounts of lipids on the L_α to H_{II} phase transition: DIM (at 1 mol%, 2.5 mol% and 5 mol%), tripalmitin (at 2.5 mol% and 5 mol%), dilinoleyl-phosphatidylethanolamine (DLiPE, at 5 mol%). We measured ^{31}P NMR spectra every two degrees between 282 K and 324 K and deconvoluted these spectra (see Methods section) to obtain the proportion of lipids in the L_α and H_{II} phase. This analysis was performed both on the PC and the PE peak so that the percentage of the two phases could be obtained independently for these two lipids. At each temperature, the PE peak displayed a higher amount of H_{II} phase than the PC peak in the same lipid preparation, in agreement with the propensity of DOPE molecules to favor and to accumulate in the H_{II} phase. Table S2 shows a subset of the spectra that have been acquired and analysed.

Table S1. Summary of Molecular Dynamics simulations

Systems	Granularity	Number of Particles	Duration (µs)
1 DIM	AT	294	0.04
1 DIM + 300 POPC + Waters	AT	79977	0.8
1 DIM + 400 POPC + Waters (DIM parametrization)	CG	13450	3
4 DIM + 400 POPC + Waters (~1% DIM) 310K	CG	13511	3
8 DIM + 400 POPC + Waters (~2% DIM) 310K	CG	13502	3
16 DIM + 400 POPC + Waters (3.8% DIM) 310K	CG	13521	3
32 DIM + 400 POPC + Waters (7.4% DIM) 310K	CG	13491	3
1248 SOPC + Waters (SOPC 310K, Lamellar)	CG	17982	3
1248 DOPE + Waters (DOPE 350K, Hexa.)	CG	16682	3
430 POPC + Waters 310K	CG	9835	3
616 SOPC+ 1880 DOPE + Waters (SOPC-DOPE 3:1 280K to 350K)	CG	37584	3x8
64 DIM + 616 SOPC+ 1880 DOPE + Waters (2.5% DIM SOPC-DOPE 3:1 280K to 350K)	CG	37320	3x8
128 DIM + 616 SOPC+ 1880 DOPE + Waters (5% DIM SOPC-DOPE 3:1 280K to 350K)	CG	38856	3x8
64 DIM + 312 SOPC+ 304 LysoPC + 1880 DOPE + Waters (2.5% DIM SOPC-DOPE 3:1 + 10% LysoPC 280K to 350K)	CG	36104	3x8
1216 POPC + 912 POPE + 608 CHOL + 304 DPSM + Waters (POPC:POPE:SM:CHOL 280K to 350K)	CG	36756	3x8
1216 POPC + 912 POPE + 608 CHOL + 304 DPSM 152 DIM (5%) + Waters (POPC:POPE:SM:CHOL + 5% DIM 280K to 380K)	CG	38484	3x11
2128 POPE + 608 CHOL + 304 DPSM + Waters (POPE:SM:CHOL 280K to 350K)	CG	36756	3x8
2128 POPE + 608 CHOL + 304 DPSM + 152 DIM (5%) + Waters (POPE:SM:CHOL + 5% DIM 280K to 350K)	CG	38484	3x8
1216 POPC + 912 POPE + 608 CHOL + 304 DPSM + 152 DIM (5%) + Waters 310K	CG	79363	10
1216 POPC + 912 POPE + 608 CHOL + 304 DPSM + 76 DIM (2.5%) + Waters 310K	CG	77539	10

Table S2. ^{31}P NMR parameters obtained on several lipids and lipid mixtures at various temperatures.
The spectra were acquired on fully hydrated multilamellar vesicles, at 2 kHz spinning rate. The CSA parameter $\Delta\delta = \delta_{//} - \delta_{\perp}$ was calculated from the spinning sideband manifold, using the solid line shape analysis tool of Topspin 3.5. The ^{31}P isotropic chemicals shifts were – 1.00 ± 0.02 ppm for the phosphatidyl choline head group (in SOPC) and – 0.27 ± 0.02 ppm for the phosphatidyl ethanolamine head group (in DOPE).

Sample composition	Temperature K	Phase	Phase %	$\Delta\delta$ (± 0.2 ppm)	Linewidth (Hz)
POPC	278	Lα	100	50,6	57
	293	Lα	100	48,2	50
	313	Lα	100	47,3	45
SOPC	293	Lα	100	49,6	50
	303	Lα	100	48,8	45
	313	Lα	100	46,7	59
	333	Lα	100	45,0	60
DOPE	278	HII	100	-22,2	131
	288	HII	100	-22,1	90
	293	HII	100	-22,1	85
	303	HII	100	-21,3	60
	313	HII	100	-21,2	55
	323	HII	100	-20,1	53
	333	HII	100	-20,1	50
DOPE SOPC 9:1	293	Lα PC	73	48,9	45
		Lα PE	59	43,3	45
		HII PC	27	-24,5	45
		HII PE	41	-21,6	45
DOPE SOPC 5:1	293	Lα PC	98	48,9	45
		Lα PE	81	43,3	45
		HII PC	2	-24,5	45
		HII PE	19	-21,6	45
DOPE SOPC 3:1	293	Lα PC	96	48,9	45
		Lα PE	80	43,3	45
		HII PC	4	-24,5	45
		HII PE	20	-21,6	45
DOPE SOPC 1:1	293	Lα PC	96	48,9	40
		Lα PE	78	43,3	40
		HII PC	4	-24,5	40
		HII PE	22	-21,6	40
POPC-POPE-SM-Chol 4:3 :1 :2	284	Lα PC	100	53,5	60
		Lα PE	100	42,9	60
	293	Lα PC	100	51,0	60
		Lα PE	100	42,3	60
	314	Lα PC	100	46,4	80
		Lα PE	100	40,1	80
	324	Lα PC	100	43,5	80
		Lα PE	100	39,2	80
POPE-SM-Chol 7 :1 :2	284	gel PE	100	47,9	130
	293	gel PE	100	43,2	100
	314	gel PE	100	39,3	100
	324	Lα PE	100	39,6	45

Table S3. Lamellar to inverted hexagonal phase transition fitting from ^{31}P NMR data and CG simulations. As described in the Supplementary Material section, both NMR and CG-derived temperature-dependent data have been fitted by a sigmoidal phase transition function in order to obtain T_{50} as well as A_0 and k. T_{50} is the phase transition midpoint temperature, A_0 the initial lamellar phase contribution and k is proportional to the slope of the function at T_{50}. For each tested lipid composition, their values are indicated together with their 95% confidence intervals ($CI_{95\%}$) as determined from the fitting procedure. Coefficient of determination (R^2), degrees of freedom and standard deviation of the residuals (Sy.x) are also indicated for each fitting result.

^{31}P NMR+											
Conditions			R^2	Degrees of freedom	Sy.x	A_0 (%)		k (K^{-1})		T_{50} (K)	
DOPE /SOPC	Added lipid					Value	$CI_{95\%}$	Value	$CI_{95\%}$	Value	$CI_{95\%}$
3:1	5% DIM	PC	0.99	18	3.6	99.4	± 3.1	-0.32	± 0.05	305.3	± 0.5
		PE	0.99	18	2.55	84.7	± 2.1	-0.40	± 0.05	303.5	± 0.4
3:1	2.5% DIM	PC	0.99	18	4.26	96.4	± 4.3	-0.23	± 0.04	306.5	± 0.9
		PE	0.99	18	2.69	87,0	± 2.7	-0.26	± 0.03	304.5	± 0.5
3:1	1% DIM	PC	0.98	18	4.91	99.2	± 3.3	-0.27	± 0.06	315.0	± 0.7
		PE	0.98	18	4.08	86.8	± 3.8	-0.19	± 0.04	311.3	± 1.0
3:1	5% DLiPE	PC	0.98	18	4.25	90.9	± 2.3	-0.51	± 0.12	317.0	± 0.5
		PE	0.99	18	2.91	83.4	± 1.7	-0.42	± 0.07	316.0	± 0.4
3:1	5% TAG	PC	0.99	18	1.90	96.2	± 3.2	-0.10	± 0.02	321.6	± 0.9
		PE	0.98	18	1.65	76.3	± 1.8	-0.13	± 0.02	321.8	± 0.8
3:1	2.5% TAG	PC	0.97	18	1.91	116.7	± 14.6	-0.04	± 0.02	329.5	± 3.5
		PE	0.98	18	1.32	94.7	± 11.9	-0.04	± 0.02	330.6	± 3.6
5:1	-	PC	0.99	17	3.27	100.8	± 1.2	-0.33	± 0.04	314.5	± 0.4
		PE	0.99	17	3.09	88.3	± 2.2	-0.31	± 0.05	310.6	± 0.5
5:1	5% LysoPC	PC	0.98	17	3.63	101.0	± 2.4	-0.30	± 0.05	316.8	± 0.5
		PE	0.99	17	2.72	93.5	± 1.9	-0.30	± 0.04	313.8	± 0.4
3:1	2.5% DIM + 5% LysoPC	PC	0.97	17	4.69	93.6	± 3.5	-0.24	± 0.05	313.6	± 0.9
		PE	0.98	17	3.63	81.4	± 3.5	-0.18	± 0.03	311.7	± 1.0
3:1	2.5% DIM + 10% LysoPC	PC	0.99	17	2.95	102.3	± 3.7	-0.11	± 0.04	329.3	± 3.6
		PE	0.98	17	3.15	83.7	± 3.9	-0.12	± 0.03	321.2	± 1.5
PE-chol-SM	5% DIM	PE	0.99	5	3.19	101.5	± 5.78	-0.73	± 0.18	318.0	± 0.4
CG simulations											
Conditions			R^2	Degrees of freedom	Sy.x	A_0 (%)		k (K^{-1})		T_{50} (K)	
DOPE /SOPC	Added lipid					Value	$CI_{95\%}$	Value	$CI_{95\%}$	Value	$CI_{95\%}$
3:1	5% DIM	PC	0.99	4	3.36	92.4	± 6.59	-0.57	± 1.22	308.1	± 4.3
		PE	0.99	4	3.31	86.3	± 6.42	-0.51	± 1.04	308.7	± 2.9
3:1	2.5% DIM	PC	0.99	5	4.91	96.3	± 6.67	-0.27	± 0.11	324.8	± 2.2
		PE	0.99	5	5.79	93.7	± 8.92	-0.17	± 0.08	324.1	± 3.4
3:1	2.5% DIM + 10% LysoPC	PC	0.98	8	6.01	88.6	± 5.66	-0.56	± 1.04	342.5	± 4.9
		PE	0.97	8	7.99	84.8	± 7.56	-0.49	± 1.00	342.2	± 4.9
PE-chol-SM	5% DIM	PE	0.97	6	6.54	100	-*	-1.38	-*	313	-*
PC-PE-chol-SM	5% DIM	PE+PC	0.96	8	8.53	100	± 9.64	-0.10	± 0.05	352.6	± 5.6

+ Raw and processed data are available at https://github.com/MChavent

* Due to the lack of sampling points to pass from the lamellar to hexagonal transition regime, the CI95% values are not reported here and the T_{50} value must be considered qualitatively.

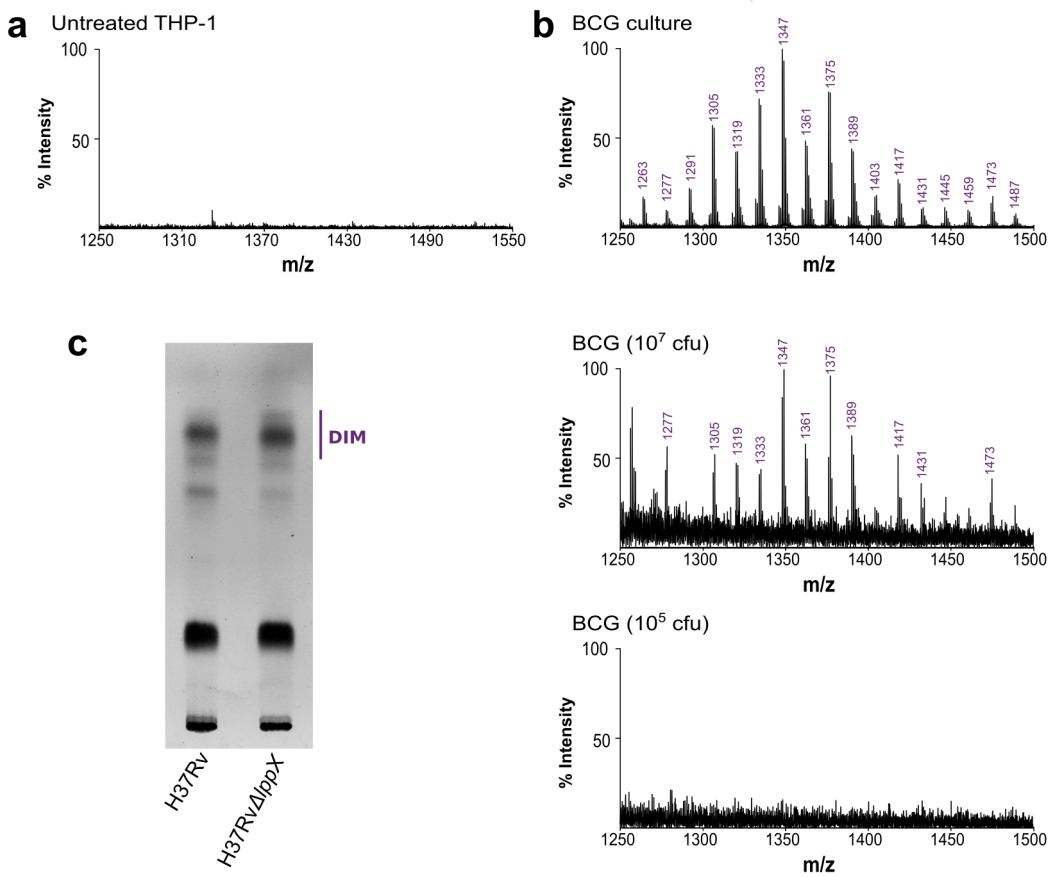

Fig. S1. DIM lipids are transferred to macrophage membranes. (**a**) MALDI-TOF spectrum of untreated THP-1 membrane fractions centered on the m/z region where DIM are expected. (**b**) MALDI-TOF spectra of lipid extracts from BCG stock culture and dilutions to 10^7 resp. 10^5 cfu. At 10^5 cfu, the concentration of DIM is below the MALDI-TOF detection threshold. (**c**) Thin layer chromatography analysis (phosphomolybdate staining) of lipids extracted from the WT H37Rv and H37Rv *ΔlppX* strains by the Bligh and Dyer method, showing that the mutant produces a similar amount of DIM as the WT strain.

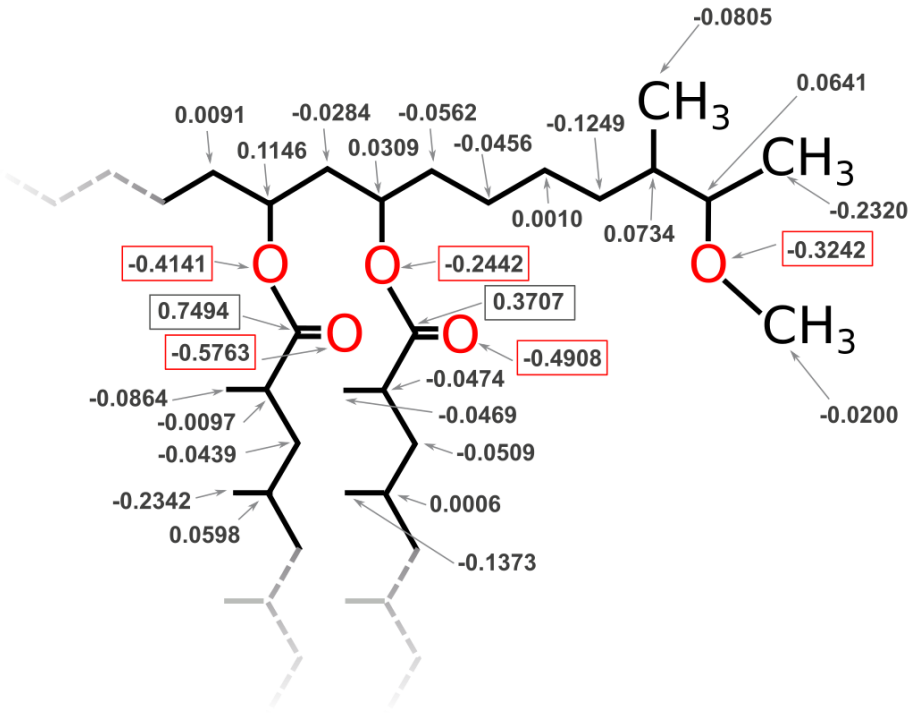

Fig. S2. DIM partial charges. Partial charges for the DIM core calculated using the RESP method (see Methods section). For the framed charge values, significant differences were observed compared to the Lipid14 parameters. For the remaining atoms, calculated charges are closed to the ones proposed by standard force fields such as Lipid14. Coordinate and topology are available at the address: https://github.com/MChavent.

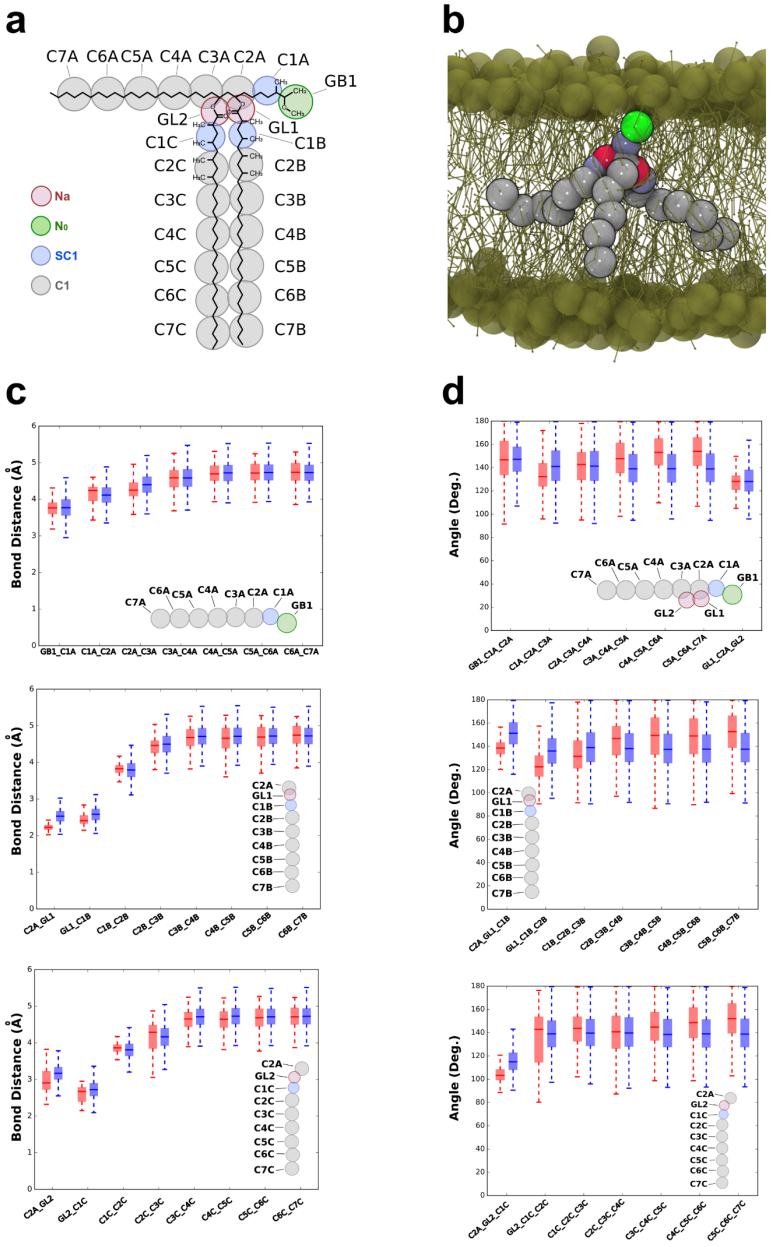

Fig. S3. DIM coarse grained model parametrization. (**a**) Mapping between chemical structure and coarse grained model for the DIM molecule. (**b**) DIM molecule in a POPC bilayer. DIM particles are colored as in (a). POPC phosphate particles are displayed in tan spheres. (**c**) Bond length distributions for atomistic (red) and coarse grained (blue) simulations for the phthiocerol moiety and the two mycocerosate tails. (**d**) Angle distributions for atomistic (red) and coarse grained (blue) simulations for the phthiocerol moiety and the two mycocerosate tails.

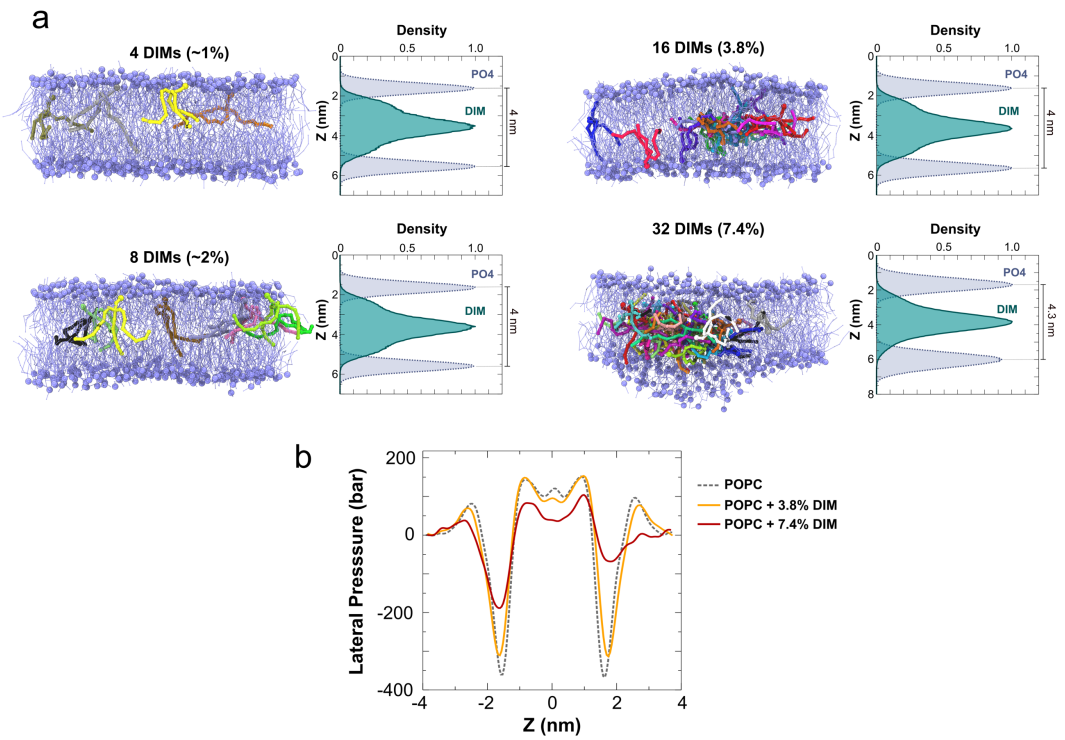

Fig. S4. DIM aggregation in a POPC bilayer. (a) Coarse grained model of DIM molecules at different concentrations embedded in a POPC bilayer (see Table S1 for more details). POPC phosphate particles are depicted as blue spheres. On the right, density of DIM lipids and phosphate head groups. Increasing the concentration of DIM molecules drove the DIM aggregation in the inter-leaflet space. At a molar concentration of DIM close to 7%, the DIM aggregation started to increase the POPC membrane thickness. **(b)** lateral pressure profile for POPC bilayer without and with the addition of 3.8% or 7.4% of DIM lipids.

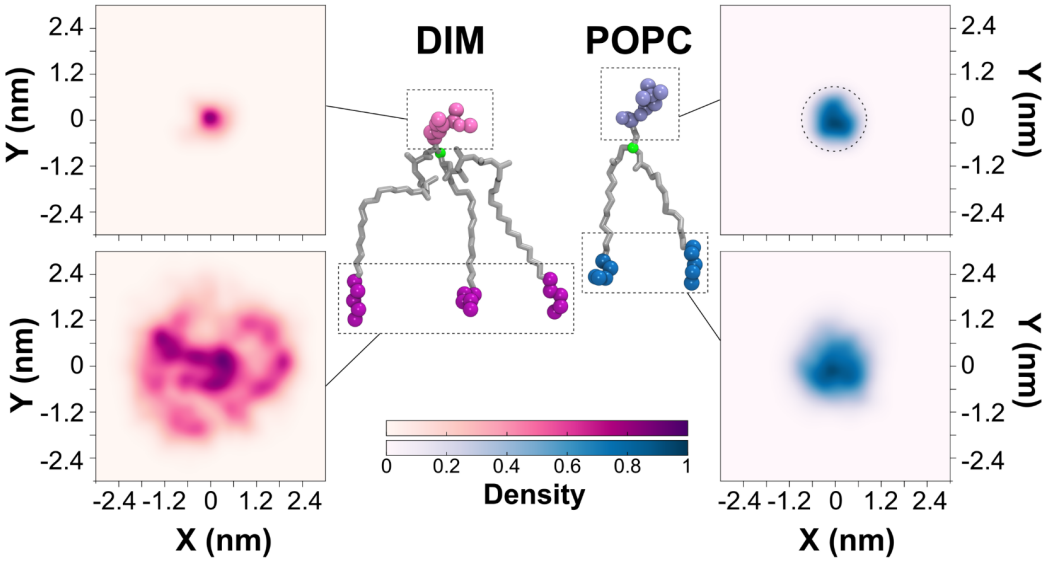

Fig. S5. Molecular shape of DIM lipids in a POPC bilayer (AT). 2D density projections of DIM and POPC extremities extracted from atomistic simulations (see **Fig. 2a**). The densities highlight the conical (resp. cylindrical) shape of the DIM (resp. POPC) molecule. Particles depicted in green were used to center the molecules. See also Figure 2 for equivalent results for coarse grained simulations.

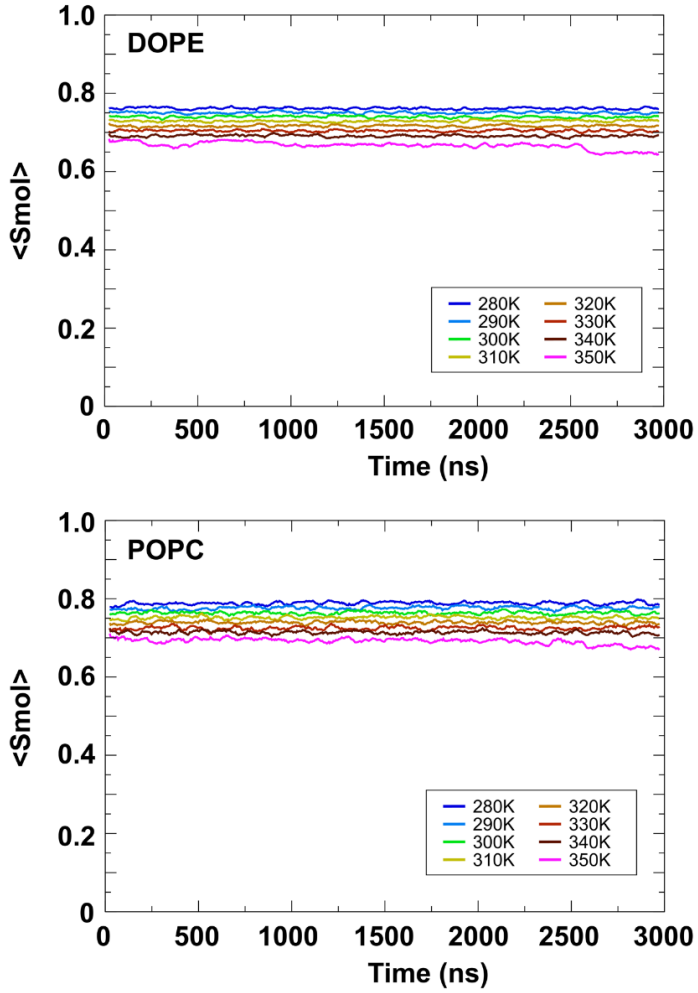

Fig. S6. 3:1 DOPE-SOPC lipid mixture displays a stable lamellar phase at different temperatures in CG simulations. Averaged reorientation of the molecular director with respect to the bilayer normal (Smol) for the 3:1 DOPE-SOPC lipid mixture taken during the course of the 3 µs CG simulations (see **Fig. 3b** for an illustration of the system at 320 K). Smol = $< 3\cos^2\theta - 1 /2 >$ with θ the angle between the lipid principal axis and the membrane normal. Smol values for DOPE molecules are slightly lower than the ones for SOPC molecules. This may highlight a higher propensity of DOPE molecules to prefer the non-lamellar phase in comparison of SOPC molecules as seen in NMR experiments (see **Fig. 3c**).

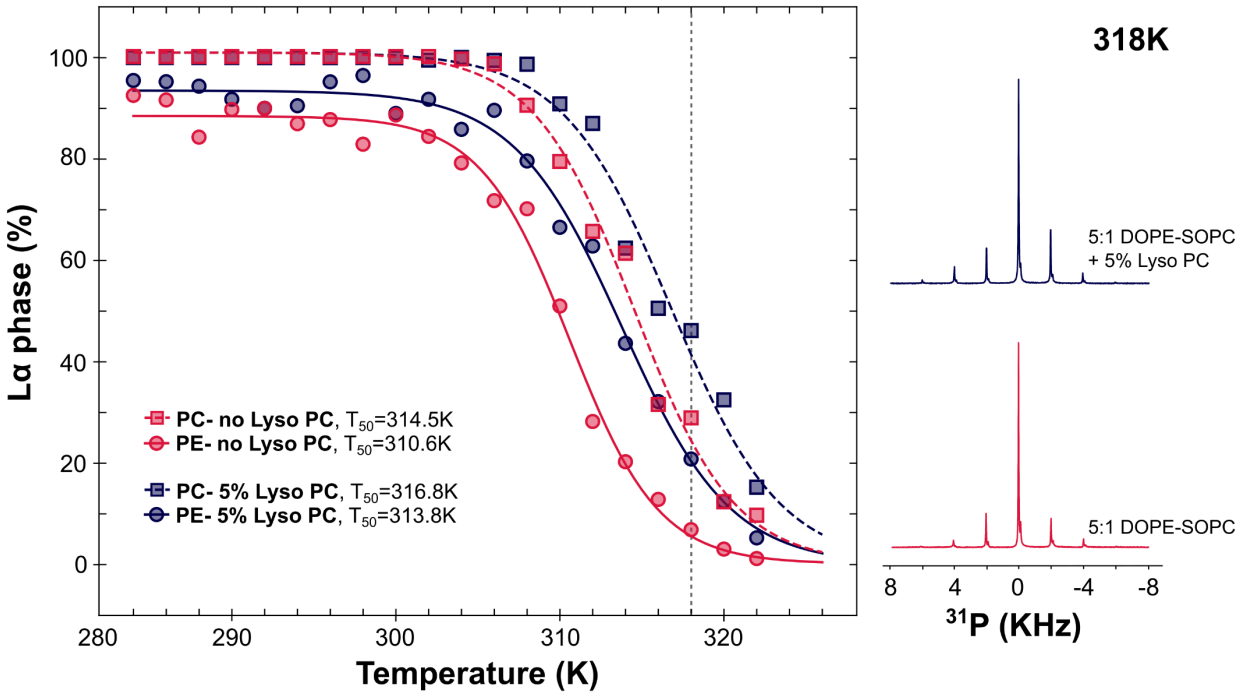

Fig. S7. LysoPC lipids shift the phase transition of a 5:1 DOPE-SOPC mixture. Left, evolution of Lα to H_{II} phase for the DOPE and SOPC molecules as a function of the temperature with and without addition of 5% of lysoPC lipids. For clarity, error bars were omitted. As seen in **Fig. 3** (see also Methods section), the error was evaluated to +/- 5%. The dashed line highlights the different temperature points obtained for the spectra shown on the right. Right, ^{31}P NMR spectra for the lipids in a 5:1 DOPE-SOPC lipid mixture with and without addition of 5% of lysoPC at 318 K.

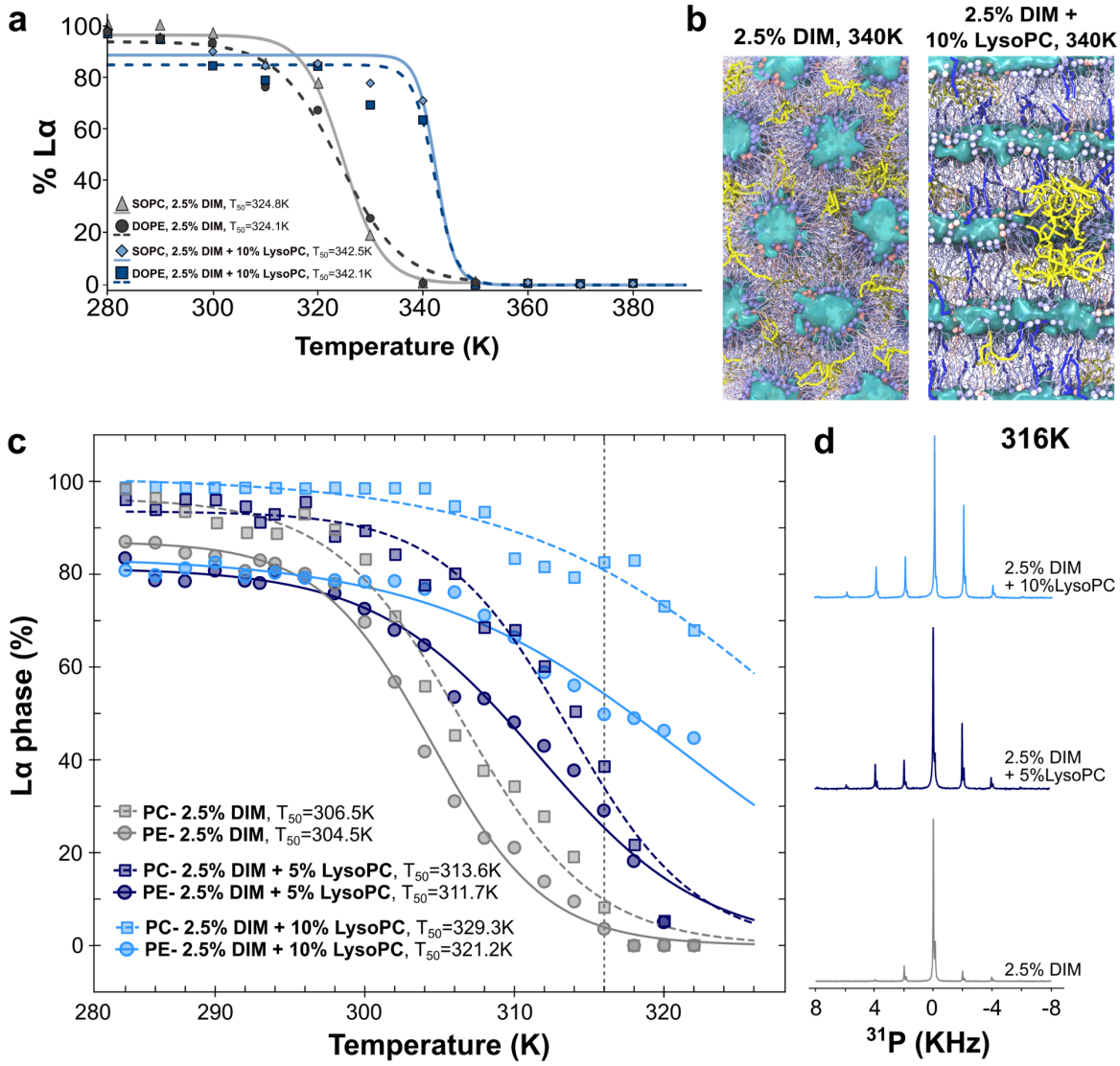

Fig. S8. LysoPC lipids modulate the non-bilayer induction of DIM lipids in a 3:1 DOPE-SOPC mixture. (**a**) SOPC and DOPE phase transitions calculated from CG-MD simulations with addition of 2.5% of DIM (as presented in **Fig. 3d**) and with addition of 2.5% of DIM and 10% of lysoPC lipids. The addition of 10% of lysoPC lipids shifts the phase transition to higher temperature values highlighting the modulation of the action of DIM by lysoPC molecules. (**b**) Coarse grained models of phase transition for a 3:1 mixture of DOPE-SOPC containing 2.5% of DIM or 2.5% of DIM and 10% of lysoPC. The addition of lysoPC limits the formation and expansion of stalks in simulations. Snapshots taken at the end of the 3μs simulation for a temperature of 340 K. POPC lipids colored in red. DOPE molecules colored in blue. DIM molecules colored in yellow. LysoPC molecules colored in dark blue. Water molecules represented as a blue surface. LysoPC molecules are homogeneously spread throughout the membrane and not concentrated around DIM lipids. (**c**) Evolution of the L_α to H_{II} phase for the DOPE and SOPC molecules as a function of the temperature for a 3:1 DOPE-SOPC mixture containing 2.5% of DIM lipids with different concentrations of lysoPC lipids. For clarity, error bars were omitted. As seen in **Fig. 3** (see also Methods section), the error was evaluated to +/- 5%. The dashed line highlights the different temperature points obtained for the spectra described on the right. Right, ^{31}P NMR spectra for the lipids in a 3:1 DOPE-SOPC lipid mixture containing 2.5% of DIM lipids with the addition of different concentrations of lysoPC at 316 K.

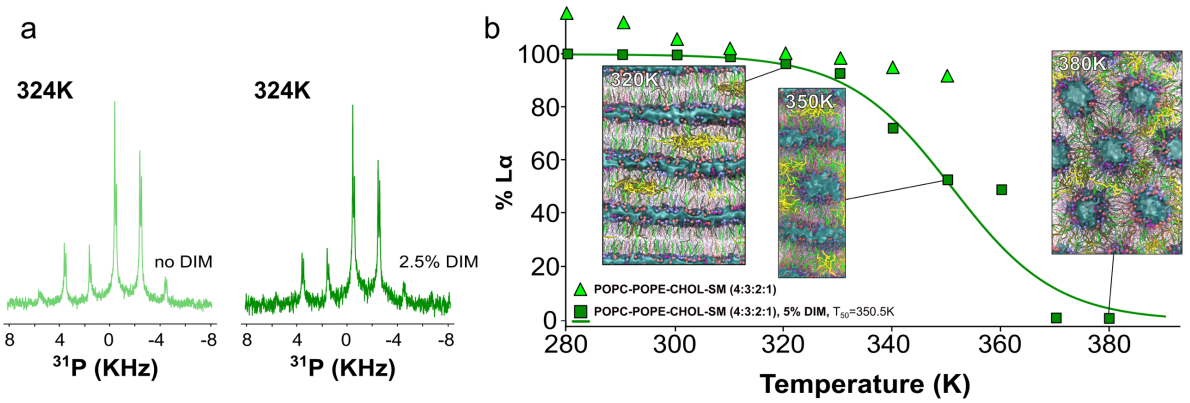

Fig. S9: DIM may induce a H_{II} phase at high temperature for a macrophage-membrane-like lipid composition. (a) The ^{31}P NMR spectra for POPC-POPE-Chol-SM (ratio 4:3:2:1) were acquired between 284 K and 324 K (see also Table S2). For this range of temperatures, all spectra indicated a lamellar phase equivalent to the spectrum at 324 K. Only 2.5% of DIM was soluble in this lipid mixture. It was not possible to reach higher temperatures due to sample degradation above 324 K. **(b)** Phase transitions calculated from CG-MD simulations with 5% of DIM included in a symmetric bilayer constituted by POPC-POPE-Chol-SM (ratio 4:3:2:1). The full transition is reached at a very high temperature (370 K) and the phase mid-point temperature is 350.5K. The same lipid mixture without DIM does not start to transit to the H_{II} phase in the range of temperature studied: 280 K to 350 K. In this case, at low temperature, some values of the percentage of Lα are higher than 100%, which may be due to the presence of cholesterol creating a different distribution of lipid orientations than in the SOPC bilayer at 310 K taken as the lamellar reference. Snapshots shown are taken at the end of the 3 μs simulations. POPC molecules colored in red. POPE molecules colored in blue. Cholesterol molecules colored in green. Sphingomyelin molecules colored in purple. DIM molecules colored in yellow. Water molecules represented as a blue surface.

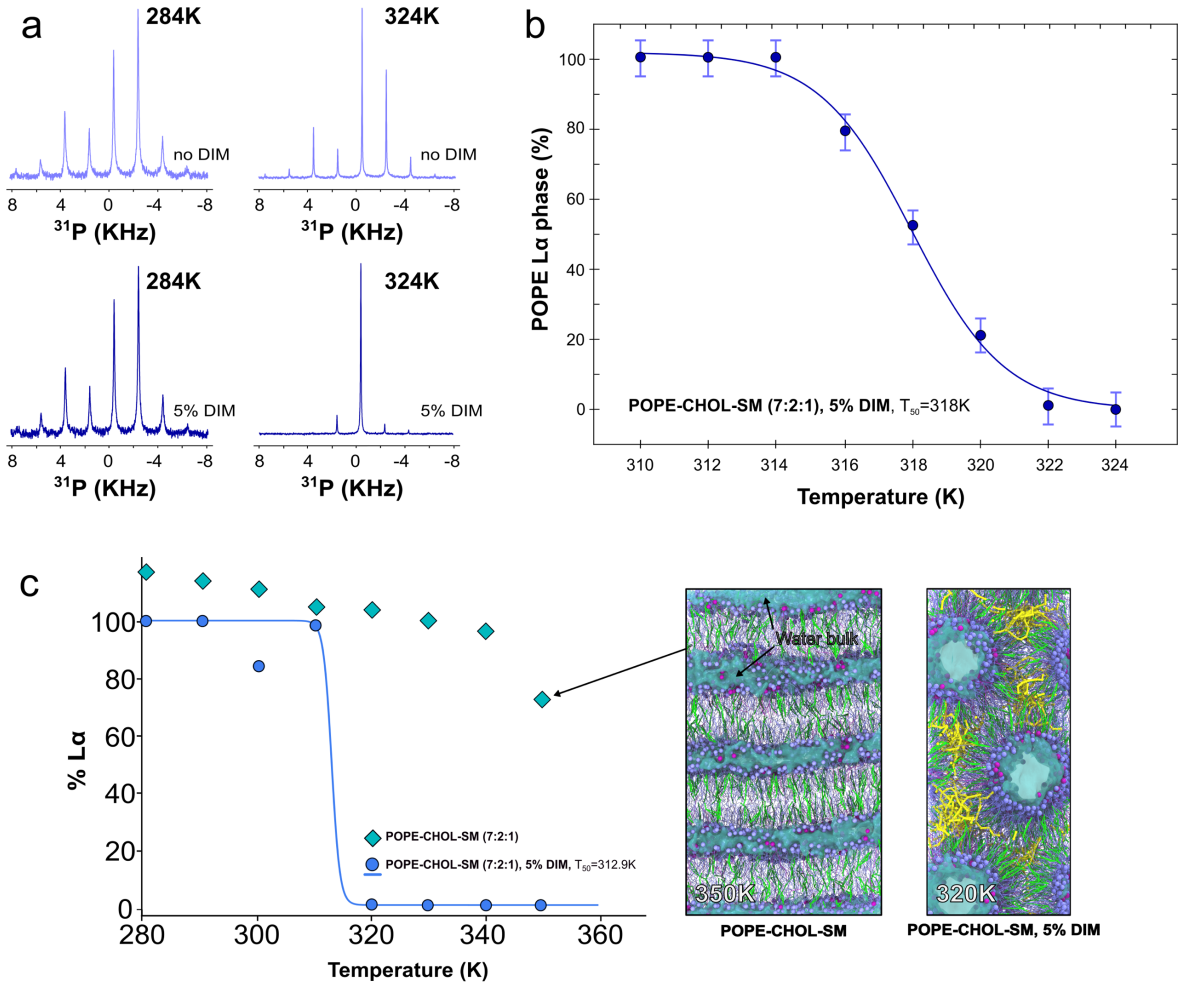

Fig. S10: DIM induce a H_{II} phase in a complex lipid composition of POPE-Chol-SM (ratio 7:2:1). **(a)** The ^{31}P NMR spectra for POPE-Chol-SM (ratio 7:2:1) were acquired between 284 K and 324 K (see also Table S2). Here, we focus on the transition from 310 K to 324 K. The transition mid-point temperature is 318K. **(b)** ^{31}P NMR spectra at different temperatures for POPE-Chol-SM (ratio 7:2:1) without DIM or containing 5% of DIM. **(c)** Phase transitions calculated from CG-MD simulations with 5% of DIM included in a symmetric bilayer constituted of POPE-Chol-SM (ratio 7:2:1). The transition occurs between 310 K and 320 K. For comparison, the same lipid mixture without DIM only starts to transit at 350 K. In this case, at low temperature, some values of Lα are higher than 100%, which may be due to the presence of cholesterol creating a different distribution of lipid orientations than in the SOPC bilayer at 310 K taken as the lamellar reference. Snapshots shown are taken at the end of the 3 µs simulations. POPE molecules colored in blue. Cholesterol molecules colored in green. Sphingomyelin molecules colored in purple. DIM molecules colored in yellow. Water molecules represented as a blue surface.

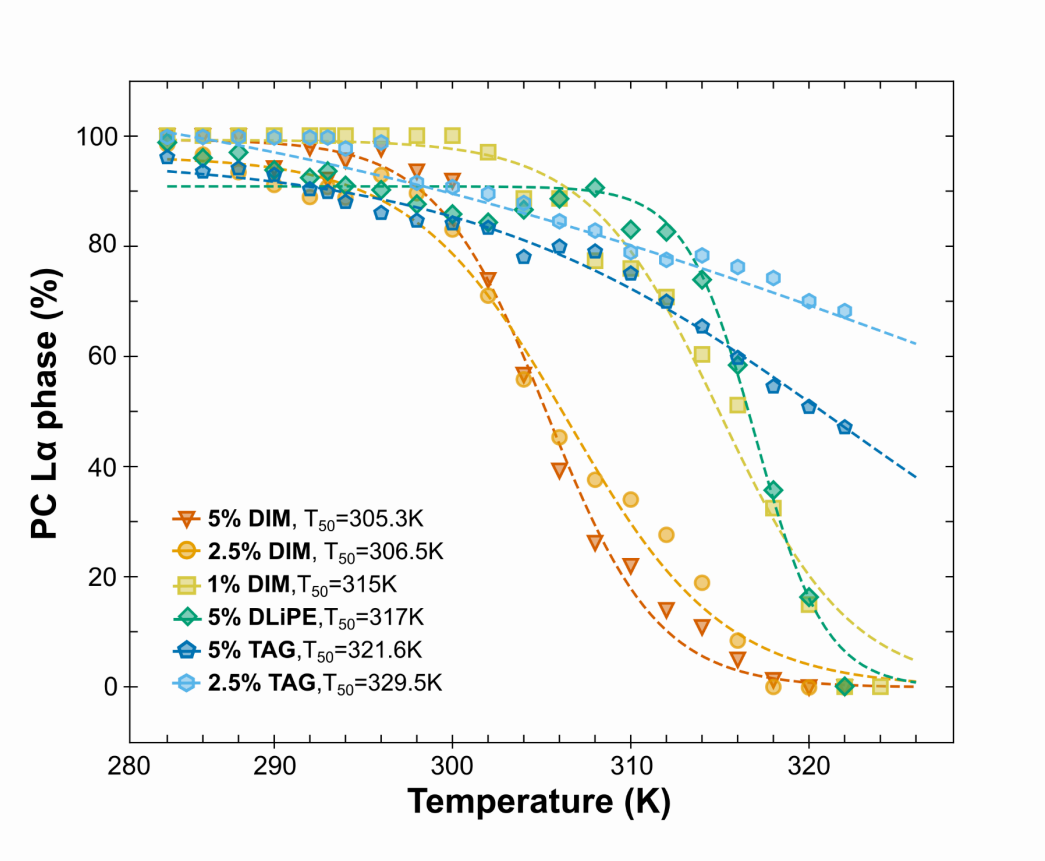

Fig. S11. DIM potency to induce non-bilayer phase compared with lipids of different shapes (L_α transition of SOPC). Evolution of the percentage of L_α phase for the SOPC molecules as a function of temperature upon incorporation of different concentrations of DIM, DLiPE and TAG in a (3:1) DOPE/SOPC mixture (see also **Fig. 4** for the corresponding curves for DOPE molecules). For clarity, error bars were omitted. As seen in **Fig. 3** (see also Methods), the error was evaluated to +/- 5%.

Movie S1: CG-MD simulation of the L_{α}-to-H_{II} phase transition of a DOPE/SOPC (3:1) mixture induced by DIM lipids (red). Water molecules are depicted in transparent blue. For DOPE and SOPC lipids, the polar head group particle PO4 is depicted in green while ester particles (GL1 and GL2) are depicted in gray. For clarity reasons, the SOPC and DOPE acyl chains were removed.

Supplementary References:

1. Laval F, Lanéelle MA, Déon C, Monsarrat B, Daffé M (2001) Accurate molecular mass determination of mycolic acids by MALDI-TOF mass spectrometry. *Anal Chem* 73(18):4537–4544.
2. Simeone R, et al. (2007) Molecular dissection of the biosynthetic relationship between phthiocerol and phthiodiolone dimycocerosates and their critical role in the virulence and permeability of Mycobacterium tuberculosis. *FEBS J* 274(8):1957–1969.
3. Astarie-Dequeker C, et al. (2009) Phthiocerol dimycocerosates of M. tuberculosis participate in macrophage invasion by inducing changes in the organization of plasma membrane lipids. *PLoS Pathog* 5(2):e1000289.
4. Pelicic V, et al. (1997) Efficient allelic exchange and transposon mutagenesis in Mycobacterium tuberculosis. *Proc Natl Acad Sci USA* 94(20):10955–10960.
5. Arbués A, et al. (2016) Trisaccharides of Phenolic Glycolipids Confer Advantages to Pathogenic Mycobacteria through Manipulation of Host-Cell Pattern-Recognition Receptors. *ACS Chem Biol* 11(10):2865–2875.
6. Rhoades E, et al. (2003) Identification and macrophage-activating activity of glycolipids released from intracellular Mycobacterium bovis BCG. *Mol Microbiol* 48(4):875–888.
7. Bligh EG, Dyer WJ (1959) A rapid method of total lipid extraction and purification. *Can J Biochem Physiol* 37(8):911–917.
8. Dickson CJ, et al. (2014) Lipid14: The Amber Lipid Force Field. *J Chem Theory Comput* 10(2):865–879.
9. Wang J, Wolf RM, Caldwell JW, Kollman PA, Case DA (2004) Development and testing of a general amber force field. *J Comput Chem* 25(9):1157–1174.
10. Bayly CI, Cieplak P, Cornell W, Kollman PA (1993) A well-behaved electrostatic potential based method using charge restraints for deriving atomic charges: the RESP model. *The Journal of Physical Chemistry* 97(40):10269–10280.
11. Dupradeau F-Y, et al. (2010) The R.E.D. tools: advances in RESP and ESP charge derivation and force field library building. *Phys Chem Chem Phys* 12(28):7821–7839.
12. Singh UC, Kollman PA (1984) An approach to computing electrostatic charges for molecules. *J Comput Chem* 5(2):129–145.
13. Besler BH, Merz KM, Kollman PA (1990) Atomic charges derived from semiempirical methods. *J Comput Chem* 11(4):431–439.
14. Marrink S-J, Mark AE (2004) Molecular view of hexagonal phase formation in phospholipid membranes. *Biophys J* 87(6):3894–3900.
15. Czaplicki J, Cornélissen G, Halberg F (2006) GOSA, a simulated annealing-based program for global optimization of nonlinear problems, also reveals transyears. *Journal of applied biomedicine* 4(2):87–94.
16. Cullis PR, De Kruijff B (1978) Polymorphic phase behaviour of lipid mixtures as detected by 31P NMR. Evidence that cholesterol may destabilize bilayer structure in membrane systems containing phosphatidylethanolamine. *Biochim Biophys Acta* 507(2):207–218.
17. Dufourc EJ, Mayer C, Stohrer J, Althoff G, Kothe G (1992) Dynamics of phosphate head groups in biomembranes. Comprehensive analysis using phosphorus-31 nuclear magnetic resonance lineshape and relaxation time measurements. *Biophys J* 61(1):42–57.
18. Moran L, Janes N (1998) Tracking Phospholipid Populations in Polymorphism by Sideband Analyses of 31P Magic Angle Spinning NMR. *Biophys J* 75(2):867–879.
19. Dekker CJ, Geurts van Kessel WSM, Klomp JPG, Pieters J, De Kruijff B (1983) Synthesis

and polymorphic phase behaviour of polyunsaturated phosphatidylcholines and phosphatidylethanolamines. *Chemistry and Physics of Lipids* 33(1):93–106.